Int. J. Solids Structures, 1978, Vol. 14, pp. 141–152. Pergamon Press. Printed in Great Britain

STRESS-WAVE DETECTION OF AN EDGE CRACK IN AN ELASTIC ROD

JAMES W. PHILLIPS
Department of Theoretical and Applied Mechanics, University of Illinois at Urbana-Champaign, Urbana, IL 61801, U.S.A.

ARTHUR F. MAK
The Technological Institute, Northwestern University, Evanston, IL 60201, U.S.A.

and

NOEL E. ASHBAUGH
Systems Research Laboratories, Inc., Dayton, OH 45440, U.S.A.

(*Received* 21 *March* 1977; *revised* 2 *August* 1977)

Abstract—Mechanical stress wave propagation in a long, thin, isotropic, elastic rod containing a single transverse edge crack is studied theoretically and experimentally. It is found that one-dimensional wave theories, coupled with an effective "compliance" of the cracked region, predict reasonably well the observed dynamic strains induced by a longitudinal impact. Remote sensing of relatively deep cracks appears feasible and consequently the procedure may be useful clinically for determining the rate of healing of partially cracked bone.

1. INTRODUCTION

The nondestructive detection of flaws and cracks in materials is a subject of continuing interest to segments of the engineering community. The present study, however, was prompted by the suggestion that mechanical wave propagation techniques may be useful as a clinical procedure for determining the rate of healing of a partially cracked bone. Apparently, analyses of X-ray photographs, patient discomfort, and other clinical factors often lead to an inconclusive diagnosis regarding the extent of healing at a fracture site, and an independent procedure for determining the mechanical strength of the fracture site would be desirable. In this connection, ultrasonic methods have met with only limited success, according to Saha and Pelker[1].

In the bioengineering literature, some work has been reported on the use of stress waves to determine mechanical integrity of bone. Saha and Pelker[1] describe results of tests in which strain gages mounted on embalmed human femurs recorded the passage of impact-generated stress pulses. Buturla and Pope[2] used a two-dimensional finite-element wave propagation model to predict "wave propagation velocities", and found that mathematically simulated fractures had a small effect upon the time of transit of transverse waves through the fracture zone. They reported some correlation between their results and some non-invasive *in vivo* tests on human tibia.

Recently, Lewis[3] has used a mechanical model of a fractured bone to investigate the feasibility of a clinical procedure involving the excitation and detection of flexural waves in a bone. Lewis' model consists of two Bernoulli beams joined by a compliant element capable of sustaining shear and bending. On the basis of his results, Lewis concludes that the method may have merit, even though wave propagation in living bone is known to be more complex than that in the model he considered. On the other hand, Sonstegard and Matthews[4] have found from invasive clinical tests that the healing of fractured bone has significant effects upon the propagation of transverse-impact-generated waves through the fractured region. They conclude that the method definitely has clinical applicability and suggest that a more thorough understanding of the types of wave they monitored would be desirable.

The present study seeks to shed more light on the subject by analyzing an alternative mechanical model of a fractured bone. As in Lewis' model[3], a fractured bone is treated as two elastic bars; however, the effects of rotatory inertia, transverse shear, and longitudinal momentum are included, and a rational procedure for determining the compliance of the cracked region is introduced. Previous experience with a related problem[5] indicates the possible suitability of one-dimensional theories of wave propagation in the current study.

It is recognized at the outset that the correct modeling of bone behavior is an extremely difficult, if not impossible, task. Actual bones are inhomogeneous, nonuniform, and anelastic, and are surrounded by soft tissue having a complex mechanical behavior. Characterization of the healing process is also a subject of concern, depending upon the type of fracture. For complete fractures, Lewis' compliance model is probably more realistic than the one considered here. The overall modeling proposed in this paper serves only to determine whether or not the potential clinical application of the method for partial fractures has some rational basis in mechanics.

It is hoped that the results reported here will find application in flaw detection methods other than the particular biomechanical one which served to motivate the work.

2. WAVE PROPAGATION THEORIES

In this paper, a cracked bone is modeled as two straight, collinear, uniform, isotropic, linear elastic rods joined at a common interface. The normalized axial coordinate is designated by s, and the interface is located at $s = s_2$, as illustrated in Fig. 1(a). Within each of the rods, a combination of elementary one-dimensional longitudinal waves and one-dimensional Timoshenko-type waves is assumed to exist. If it were not for the interface, there would be no interaction at all between the longitudinal waves and the bending waves. A coupling of the two types of wave occurs at the interface.

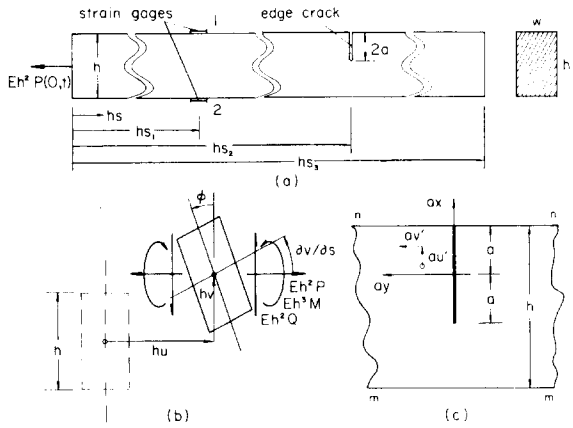

Fig. 1. Nomenclature. All quantities are dimensional as indicated.

Throughout the paper, nondimensionalized variables are employed. In connection with wave propagation, the axial coordinate s, the axial displacement u and the transverse displacement v are normalized with respect to the rod diameter (or thickness) h; the axial and transverse forces P and Q, respectively, are normalized with respect to Eh^2, where E is Young's modulus for the rod material; the bending moment M is divided by Eh^3; the cross-sectional area A and the moment of inertia I are divided by h^2 and by h^4, respectively; and time t is normalized with respect to h/c_0, where c_0 is the "bar velocity" $(E/\rho)^{1/2}$, ρ being the mass density of the rod material. Certain other variables are normalized with respect to the crack half-length, as discussed in Section 3.

Longitudinal waves

The elementary theory for longitudinal waves is used. Since the pulses employed in the experimental program are smooth and have dominant wavelengths of the order of several bar diameters, use of the elementary theory is probably justified. In this theory, the equation of motion may be written in the form

$$P_{,s} - Au_{,tt} = 0, \tag{2.1}$$

where a comma (,) denotes partial differentiation with respect to the subscripted variable. The

generalized constitutive relation is the isotropic linear elastic relation

$$P - Au_{,s} = 0. \tag{2.2}$$

Suitable differentiation and combination of (2.1) and (2.2) result in the classical wave equation $u_{,tt} - u_{,ss} = 0$, for which a solution is $u = F(s - t)$, where F is any function; this fact will be useful in the determination of the actual boundary condition imposed experimentally at $s = 0$.

Transverse bending waves

The Timoshenko theory[6] governing the transverse motion of the rod is also employed. According to this theory, the relevant equations of motion are

$$Q_{,s} - Av_{,tt} = 0 \tag{2.3}$$

and

$$M_{,s} - I\phi_{,tt} = 0, \tag{2.4}$$

where ϕ is the total rotation of a cross-section originally perpendicular to the rod axis, as illustrated in Fig. 1(b). The associated generalized constitutive relations are

$$Q - (\kappa^2 G/E)A(v_{,s} - \phi) = 0 \tag{2.5}$$

and

$$M - I\phi_{,s} = 0, \tag{2.6}$$

where κ^2 is the shear correction factor and G is the shear modulus of the rod material. In this work, a square cross-section was employed, and the value for κ^2 was taken to be $\pi^2/12$[7].

It is well known that eqns (2.3)–(2.6) may be suitably differentiated and combined into a pair of coupled second-order equations relating the displacement v and the rotation ϕ[8]. For continuous wavetrains, two frequency-dependent wavespeeds are found to exist.

It will be seen that there is no coupling between the pair of eqns (2.1), (2.2) and the set of eqns (2.3)–(2.6), i.e. longitudinal-type disturbances and bending-type disturbances propagate independently of each other in a straight rod. The same is *not* true in the case of naturally curved rods, but even for curved rods, a Timoshenko-type theory[9] that introduces no new dependent variables has been shown to describe well the propagation of mechanical pulses[10]. Thus, with only a moderate increase in the complexity of the governing equations, the restriction that the bar be straight could be removed.

3. INTERFACE MODELING

Attention is now focused on the interface containing the partial transverse crack. In keeping with the one-dimensional nature of the wave propagation theories being used, a one-dimensional "compliance" of the cracked region is sought. A two-step procedure is used to develop the necessary "compliance" terms: first, a solution is obtained to the static two-dimensional elasticity problem of a perpendicular edge crack in an infinitely long strip of finite width, subjected to known boundary conditions at infinity; then, the two-dimensional crack opening displacement distribution is "averaged" in a manner consistent with the one-dimensional theories of wave propagation. The result is a set of algebraic equations relating jumps in the one-dimensional displacements to the generalized forces acting at the interface.

Two-dimensional solution for an edge crack in an infinite strip

Consider the problem of an infinitely long strip of width h and thickness w, containing a perpendicular edge crack of length $2a$. Let the x and y coordinates for the strip be normalized with respect to the half-crack length a, as illustrated in Fig. 1(c). In the following analysis, the

u' and v' displacement components along the x and y axes, respectively, have also been normalized with respect to the half-crack length a.

The solution of the two-dimensional elasticity problem for the strip with stress-free lateral sides, *nn* and *mm* in Fig. 1(c), can be determined with the application of Fourier sine and cosine transforms; see [11]. The solution is composed of solutions to two intermediate problems. The solution to the first intermediate problem is determined for the boundary tractions at infinity on a strip which does not contain a crack. Usually, the first problem has a trivial solution, as in the case of uniaxial tension or of pure bending. The solution for the second intermediate problem (for which Fourier transforms are used) is determined for nonzero tractions specified only on the crack surfaces. The stress components for the tractions in the second problem are the negative of the stress components calculated from the first problem at the points where the crack would exist. With the principle of superposition, the solution of the original problem is the sum of the solutions to the intermediate problems.

In the present investigation, the crack-opening displacement distribution which is needed for the one-dimensional wave propagation model is obtained directly from the second intermediate problem. After application of the Fourier transforms and their inverse transforms, the derivative with respect to x of the displacement normal to the crack surface can be related directly to the traction on the crack surface by an integral of the following form:

$$\frac{1-\nu}{G}\,{}^{*}\!\int_{-1}^{+1}\frac{\partial v'(\xi,0^+)}{\partial \xi}\left(\frac{1}{\xi-x}+H(\xi,x)\right)\mathrm{d}\xi = n(x), |x|<1, \tag{3.1}$$

where ν and G are Poisson's ratio and shear modulus, respectively, of the strip material, the asterisk (*) indicates the Cauchy principal value of the integral, $H(\xi, x)$ is a kernel function which contains both the geometric and the boundary condition information on the sides of the strip, and $n(x)$ is the stress normal to the crack surface. Equation (3.1) is regarded as a preliminary result and consequently the expression for $H(\xi, x)$ will not be presented.

Applying the Cauchy principal value operator

$${}^{*}\!\int_{-1}^{+1}\left(\ldots\right)\frac{\mathrm{d}x}{x-t} \tag{3.2}$$

to both sides of (3.1) leads to a convenient expression for the numerical evaluation of the derivative of the normal displacement:

$$f(x)+\frac{1}{\pi}\int_{-1}^{+1}\frac{f(\xi)}{\sqrt{(1-\xi^2)}}[K(\xi,x;0)+(\xi,x;h')-L(\xi,x;h')]\,\mathrm{d}\xi - C = -N(x), \tag{3.3}$$

where

$$f(x)\equiv\sqrt{(1-x^2)}\,\frac{G}{1-\nu}\,\frac{\partial v'(x,0^+)}{\partial x}, \tag{3.4}$$

$$N(x)\equiv\frac{1}{\pi}\,{}^{*}\!\int_{-1}^{+1} n(t)\frac{\sqrt{(1-t^2)}}{t-x}\,\mathrm{d}t, |x|<1, \tag{3.5}$$

$h'\equiv h/a>2$,

C = unknown constant,

and $K(\xi, x; \beta)$ (where β is either 0 or h') and $L(\xi, x; h')$ are kernel functions which are discussed next.

The first kernel function in (3.3) gives the solution for a half-plane with a perpendicular edge crack at the stress-free boundary, i.e. boundary *nn* in Fig. 1(c). Similarly, the second kernel function in (3.3) is associated with a half-plane which has a stress-free boundary a distance h away from the crack tip at $x = 1$, i.e. boundary *mm* in Fig. 1(c). The third kernel in (3.3) accounts for the tractions created by the first kernel on boundary *mm* and the tractions created by the second kernel on boundary *nn*. Thus, the condition that each side of the strip is

stress-free is contained in the sum of the kernel functions. Explicit expressions for the kernel functions are:

$$K(\xi, x; \beta) = 1 - \frac{\sqrt{(\rho_1\rho_2)}}{\rho_3} - 2\left((1-\beta-\xi)\frac{\partial}{\partial\xi}\right)^2\left(\frac{\sqrt{(\rho_1\rho_2)}}{\rho_3}\right),$$

where

$$\rho_1 = 1 - 2\beta - \xi,$$
$$\rho_2 = 3 - 2\beta - \xi,$$
$$\rho_3 = 2 - 2\beta - \xi - x,$$

and

$$L(\xi, x; h') = -x\int_0^\infty \bar{K}(\xi, t, \eta; h')\,\mathrm{d}\eta + \frac{1}{\pi}\int_{-1}^{+1}\frac{\sqrt{(1-t^2)}}{t-x}\left\{\int_0^\infty [\bar{K}(\xi, t, \eta, h') - \bar{K}(\xi, x, \eta; h')]\,\mathrm{d}\eta\right\}\mathrm{d}t, \tag{3.6}$$

where

$$\begin{aligned}\bar{K}(\xi, x, \eta; h') = {} & [\{[-\tfrac{1}{2} + \eta h' + \eta\xi - \eta][m'(2 - m' + 4\eta^2h'^2)(-4 + 2\eta x - 2\eta)m_x - (4 + 2\eta x - 2\eta)p_x] \\ & + [(1 + 2\eta h')(\eta\xi - \eta) + 2\eta^2h'^2][m'(2 - m' \oplus 4\eta^2h'^2)m_x + (3 + 2\eta x - 2\eta)p_x] \\ & + [\tfrac{1}{2} - \eta\xi - \eta][m'(-4 + 2\eta x - 2\eta)m_x - m'(4 \oplus 2\eta x - 2\eta)p_x] \\ & - (\eta\xi - \eta)m'[m_x + (3 + 2\eta x - 2\eta)p_x]\}m_\xi \\ & + \{[\tfrac{1}{2}(1 - m') - \eta h' - 2\eta^2h'(\xi - 1)][(-4 + 2\eta x - 2\eta)m_x - (4 + 2\eta x - 2\eta)p_x] \\ & + [(1 - m' + 2\eta h' + 4\eta^2h'^2)\eta(\xi - 1) + 2\eta^2h'^2][-m_x - (3 + 2\eta x - 2\eta)p_x]\}p_\xi] \\ & /[p' + m' - 2 - 4\eta^2h'^2],\end{aligned}$$

$$\left.\begin{aligned} m' &\equiv \exp(-2\eta h'),\ p' \equiv \exp(2\eta h'), \\ m_\gamma &\equiv \exp(-\eta\gamma + \eta) \\ p_\gamma &\equiv \exp(\eta\gamma - \eta) \end{aligned}\right\},\ \gamma = x, \xi.$$

With regard to the integrals in (3.6), it should be noted that $\bar{K} = o(1)$ as $\eta \to 0$ and $\bar{K} = o(\exp(-2))$ as $\eta \to \infty$, and that the integrand of the integral over t is continuous and differentiable at $t = x$. Various numerical integration procedures could be used to evaluate the right-hand side of (3.6). However, Gaussian quadrature was used to evaluate $f(x)$ in (3.3), and it was convenient to apply the same procedure to compute the right-hand side of (3.6). Comparison of selected numerical results for $L(\xi, x; h')$ in (3.6) with the results from specialized numerical procedures for the evaluation of the two types of integral in (3.6) yielded differences in only the fourth significant digit of the results.

Before the application of the Gaussian quadrature method, the following change of variables is made in (3.3): x is replaced by $\sin(\pi x/2)$ and ξ is replaced by $\sin(\pi\xi/2)$. Also, the constant C is determined by the additional requirement that the stresses be bounded at the point $x = 1$, $y = 0^+$. Since demanding bounded stresses at $x = 1$ is equivalent to setting $f(1) = 0$, it follows from (3.3) that C must satisfy the equation

$$\frac{1}{\pi}\int_{-1}^{+1}\frac{f(\xi)}{\sqrt{(1-\xi^2)}}[K(\xi, 1; 0) + K(\xi, 1; h') - L(\xi, 1; h') - L(\xi, 1; h')]\,\mathrm{d}\xi - C = -N(1). \tag{3.7}$$

Substracting (3.7) from (3.3), and employing the change of variables just mentioned, one finds that

$$f\left(\sin\frac{\pi}{2}x\right)+\frac{1}{2}\int_{-1}^{+1} f\left(\sin\frac{\pi}{2}\xi\right)\left[K\left(\sin\frac{\pi}{2}\xi,\sin\frac{\pi}{2}x;0\right)-K\left(\sin\frac{\pi}{2}\xi,1;0\right)\right.$$
$$+K\left(\sin\frac{\pi}{2}\xi,\sin\frac{\pi}{2}x;h'\right)-K\left(\sin\frac{\pi}{2}\xi,1;h'\right)-L\left(\sin\frac{\pi}{2}\xi,\sin\frac{\pi}{2}x,h'\right)$$
$$\left.+L\left(\sin\frac{\pi}{2}\xi,1;h'\right)\right]\mathrm{d}\xi=-N\left(\sin\frac{\pi}{2}x\right)+N(1). \tag{3.8}$$

Now let x_i and $\xi_i (i=1,\ldots,M)$ denote the M Gaussian nodes in the interval $(-1,1)$. Then the solution for $f(x)$ in (3.8) is obtained from the linear set of equations

$$\sum_{i=1}^{M} f_i A_i K_{ij} = -N_j + N(1) \qquad (j=1,\ldots,M), \tag{3.9}$$

where A_i are the Gaussian weight factors,

$$f_i = f\left(\sin\frac{\pi}{2}x_i\right),$$

$$K_{ij}=\delta_{ij}+\frac{1}{2}\left[K\left(\sin\frac{\pi}{2}\xi_i,\sin\frac{\pi}{2}x_j;0\right)-K\left(\sin\frac{\pi}{2}\xi_i,1;0\right)\right.$$
$$+K\left(\sin\frac{\pi}{2}\xi_i,\sin\frac{\pi}{2}x_j;h'\right)-K\left(\sin\frac{\pi}{2}\xi_i,1;h'\right)$$
$$\left.-L\left(\sin\frac{\pi}{2}\xi_i,\sin\frac{\pi}{2}x_j;h'\right)+L\left(\sin\frac{\pi}{2}\xi_i,1;h'\right)\right],$$

$$N_i = N\left(\sin\frac{\pi}{2}x_i\right),$$

$$\delta_{ij}=\begin{cases}1, & i=j,\\ 0, & \text{otherwise.}\end{cases}$$

For the results used in this work, M was chosen to be 40.

After the values of f_i are determined, the value of $f(x)$ for any x can be found from (3.8). In particular, $f(-1)$ gives the value of the nondimensional stress intensity factor for the crack tip at $x=-1$, $y=0$. As a check on the numerical procedure, values of the stress intensity factor for various ratios of crack length to width, $2a/h$, were compared with the results in [12]. The largest percentage difference was less than 1% for $0\le 2a/h\le 0.8$ and was less than 6% at $2a/h=0.9$. It is expected that more accurate numerical results could have been obtained for deep cracks (i.e. $2a/h\to 1^-$) by additional algebraic manipulation of the kernels in (3.8) in order to avoid the determination of differences between large numbers in the numerical evaluation of K_{ij} in (3.9).

From (3.4), the nondimensional displacement normal to the crack surface is given by

$$v'(x,0^+)=\frac{1-\nu}{G}\int_{-1}^{x}\frac{f(\xi)}{\sqrt{(1-\xi^2)}}\,\mathrm{d}\xi. \tag{3.10}$$

The integral is evaluated by approximating $f(x)$ with linear segments between the known values of $f_i (i=0,1,\ldots,M,M+1)$, where $f_0=f(-1)$ and $f_{M+1}=f(1)=0$. Then the integration of (3.10) yields

$$v'(\bar{x}_i,0^+)=\sum_{j=0}^{i-1}\left\{\left(\frac{f_j\bar{x}_{j+1}-f_{j+1}\bar{x}_j}{\bar{x}_{j+1}-\bar{x}_j}\right)(\arcsin\bar{x}_{j+1}-\arcsin\bar{x}_j)\right.$$
$$\left.-\left(\frac{f_{j+1}-f_j}{\bar{x}_{j+1}-\bar{x}_j}\right)(\sqrt{(1-\bar{x}_{j+1}^2)}-\sqrt{(1-\bar{x}_j^2)})\right\}, \quad i=1,\ldots,M+1, \tag{3.11}$$

where $\bar{x}_i = \sin(\pi/2)x_i$ $(i = 1, \ldots, M)$, $\bar{x}_0 = -1$, and $\bar{x}_{M+1} = 1$. Note that the physical displacement is obtained by multiplying v' in (3.11) by a.

There are two traction conditions at infinity which are of interest in this problem. The first is that of uniform tensile loading of magnitude σ_0, in which case

$$n(x) = -\sigma_0,$$

and $N(x)$ becomes (from (3.5))

$$N(x) = +\sigma_0 x.$$

The second is that of pure bending, where the maximum stress in the uncracked strip is σ_0. Then

$$n(x) = -\sigma_0 \frac{a}{h}\left[2x + \left(\frac{h}{2} - 2\right)\right],$$

and the associated $N(x)$ becomes

$$N(x) = +\sigma_0 \frac{a}{h}\left[2x^2 + \left(\frac{h}{a} - 2\right)x - 1\right].$$

The integral eqn (3.8) is solved numerically by Gaussian quadrature for the two cases just mentioned, and the resulting data for $f(x)$ are then used in (3.11) to yield the crack opening displacement distribution $v'(x, 0^+)$.

One-dimensional approximation

A typical result for the crack opening displacement is illustrated schematically in Fig. 2. It will be seen that the two-dimensional solution provides more information about the deformation of the cracked region than can be incorporated into the one-dimensional theories of wave propagation being employed. For this reason, a least-squares linear-fit procedure is used to determine an equivalent interface centerline separation $[u(s_2^+, t) - u(s_2^-, t)]$ and a relative interface rotation $[\phi(s_2^+, t) - \phi(s_2^-, t)]$ for the two generalized forces being considered in the crack-opening analysis, namely the bending moment M and the axial force P. See Fig. 2. It is assumed that the transverse displacement v and all generalized forces are continuous at $s = s_2$, and that the discontinuities in u and ϕ are not functions of the transverse shear Q. The least-squares procedure employs the Gaussian points for $v'(x, 0^+)$ in the range $-1 < x < +1$ and equally spaced (zero) values of $v'(x, 0)$ in the range $-(h/a - 2) < x < -1$, and yields time-independent values for the compliances K_{uP}, K_{uM}, $K_{\phi P}$, $K_{\phi M}$ appearing in the relations

$$\begin{aligned} \frac{1}{2}[u(s_2^+, t) - u(s_2^-, t)] &= K_{uP}P(s_2, t) - K_{uM}M(s_2, t) \\ \frac{1}{2}[\phi(s_2^+, t) - \phi(s_2^-, t)] &= -K_{\phi P}P(s_2, t) + K_{\phi M}M(s_2, t). \end{aligned} \tag{3.12}$$

It is found that the compliances are very strong functions of the relative crack depth $2a/h$, as illustrated in Fig. 3. Note that the "cross terms" K_{uM} and $K_{\phi P}$ appear to have almost equal values. Actually, on the basis of a simple two-spring model of the interface, it can be shown that the terms K_{uM} and $K_{\phi P}$ should have the same value, and in this respect the results in Fig. 3 appear to be reasonable.

4. NUMERICAL SOLUTION

Equations (2.1)–(2.6) governing the propagation of waves in each part of the bar, augmented with relations (3.12) governing the jumps in bar displacement at the interface, are amenable to solution by the method of characteristics. Although other methods of solution could be used, the method of characteristics leads to a set of ordinary differential equations that are solved by

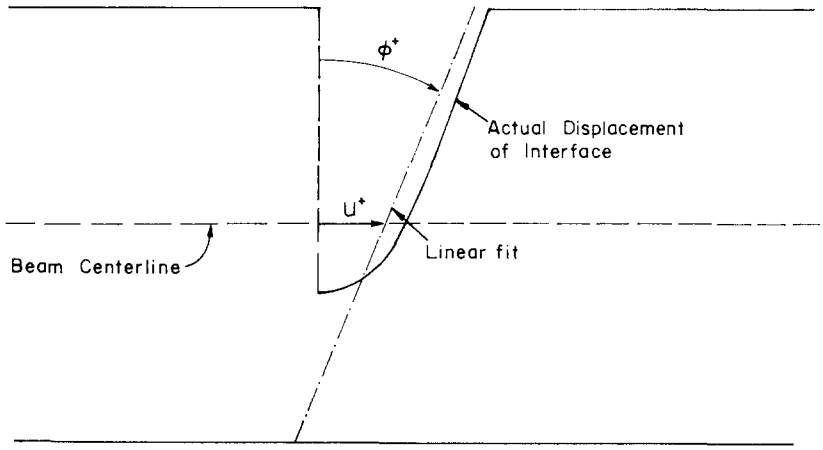

Fig. 2. Equivalent one-dimensional interface discontinuities.

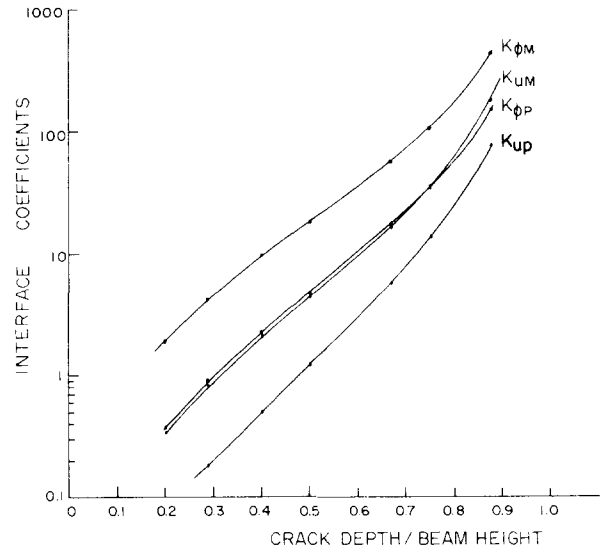

Fig. 3. Variation of the interface coefficients with the crack-depth-to-bar-thickness parameter $2a/h$.

a marching procedure[9, 14] particularly appropriate in pulse-propagation studies of this type. In addition, the interface conditions are easily treated by the method of characteristics.

Details of the solution of the Timoshenko beam equations by the method of characteristics can be found in a paper by Plass[15] and consequently the relevant equations will only be summarized here. It can be shown that there are two characteristic speeds associated with Timoshenko waves, namely

$$c_1 = 1, \qquad c_2 = \kappa\sqrt{(G/E)}.$$

Along the corresponding characteristics in st-space, the governing ordinary differential equations are

$$\begin{aligned} &dM \mp A(g/h)^2\, d\dot{\phi} \pm Q\, dt = 0 \qquad \text{for} \quad ds/dt = \pm c_1, \\ \text{and} \qquad &dQ \pm c_2 A\, d\dot{v} + A(\kappa^2 G/E)\dot{\phi}\, dt = 0 \qquad \text{for} \quad ds/dt = \pm c_2. \end{aligned} \tag{4.1}$$

In the first of (4.1), g denotes the radius of gyration of the cross-section. The characteristic speed of longitudinal waves is also c_1, and the associated equations are

$$dP \mp A\, d\dot{u} = 0 \qquad \text{for} \quad ds/dt = \pm c_1. \tag{4.2}$$

Finite-difference representations of (4.1) and (4.2) lead to a marching procedure for determining the six unknowns P, Q, M, $\dot{u}$, $\dot{v}$, $\dot{\phi}$ at regularly spaced points in st-space. The procedure is initiated by prescribing the initial values of all variables for all s; in the present analysis, these values are all zero. At the end $s = 0$, boundary conditions must be prescribed; in this problem, the generalized forces P, Q, M are given as functions of time. In keeping with the experimental procedure described in the next section, $Q(0, t)$ and $M(0, t)$ are taken to be identically zero, while (P_0, t) is inferred from the recorded traces of strain gages mounted at $s = s_1$.

At a given instant at the interface, there are twelve unknowns, namely P, Q, M, $\dot{u}$, $\dot{v}$, $\dot{\phi}$ at $s = s_2^-$ and the same set of variables at $s = s_2^+$. However, there are three finite-difference relations holding along right-running characteristics intersecting at the generic point (s_2, t) and three more along left-running characteristics intersecting at the same point; there are also four continuity conditions, as mentioned previously, and finally the two jump conditions (3.12), which complete the necessary twelve relations for this point.

As illustrated in Fig. 1(a), the entire model has some dimensionless length s_3. At the end $s = s_3$, free boundary conditions are imposed, i.e. $P(s_3, t) = 0$, $Q(s_3, t) = 0$, and $M(s_3, t) = 0$ for all t.

An incremental time step of 0.2 was used in generating the numerical results presented in this paper.

5. EXPERIMENT

As a means of evaluating the foregoing theoretical model of a cracked bone, some laboratory experiments were conducted with an aluminum bar containing a bandsawed edge crack. The bar was struck longitudinally by a shorter length of similar stock, and strain gages mounted on the bar between the impact face and the crack location monitored not only the input pulse produced during impact, but also the pulses reflected from the crack interface and from the far end of the bar.

The bar was of square cross-section, 25.4 mm on a side, and 2.13 m long. Metal-foil strain gages with a gage length of 3 mm were bonded on opposite sides of the bar at a distance of 0.71 m from the impacted end, and the crack was introduced at a distance of 1.42 m from the impacted end on the same side as gage 1, as illustrated schematically in Fig. 1(a). Strikers of various lengths were employed; all results given here are for a striker length of 0.38 m. Eccentricity of loading was minimized by machining the impact face of the instrumented bar to a slight convexity, and by supporting the striker and the bar in a series of carefully aligned padded V-grooves. The striker was accelerated by hand through a distance of approximately 0.1 m.

Potentiometer strain gage circuits[13] employing 3000 Ω ballast resistors and a 67.5 V (nominal) battery source were used to drive the 120 Ω strain gages, and the outputs were AC-coupled to separate inputs of a Tektronix type 556 dual-beam oscilloscope with type 1A7 plug-in units. A common time sweep of 0.1 ms/cm was triggered when the input pulse reached the strain gage location.

Typical oscilloscope traces are shown in Fig. 4 for a crack-depth-to-bar-thickness ratio of 0.75. The upper and lower traces in the figure correspond to gages 1 and 2, respectively, and positive signals indicate tensile strains. It will be seen that after the passage of the initial compressive strain pulse, which is approximately 0.3 ms in duration, a rather complex reflection pattern containing symmetric (longitudinal) and antisymmetric (bending) components is detected. Theoretically, for the given bar material and dimensions, the time required for a longitudinal disturbance to propagate from the strain gage location ($s = s_1$) to the crack interface ($s = s_2$) and back to the strain gage location is about 0.274 ms, and indeed the first reflections are observed to arrive at approximately this time. The earliest corresponding time for a signal reflected from the far end ($s = s_3$) is about 0.547 ms. It also happens that 0.547 ms is the earliest time that a crack-reflected pulse can reach the strain gage location after it has been reflected from the impact face ($s = 0$). Consequently, the only pulse which can be observed in the time interval between 0.274 ms and 0.547 ms after triggering is the one associated with the first reflection from the crack interface.

With these details in mind, one can see from Fig. 4 that the pulse reflected from the crack

Fig. 4. Typical strain gage responses for $2a/h = 0.75$. Common time sweep is 0.1 ms/cm. Zero levels of strain coincide with two tic-marked horizontal grid lines.

interface has both longitudinal and bending components, with the longitudinal component arriving first, as would be expected. For later times, the bending component of the crack-reflected pulse and the tensile component of the far-end-reflected pulse apparently combine to produce rather large strains.

6. RESULTS AND DISCUSSION

Oscilloscope traces have been obtained for crack-depth-to-bar-thickness ratios of 0.50, 0.75 and 0.88; they have been reproduced in solid lines in Figs. 5–7, respectively. It was found that the input strain pulse, as monitored by the strain gages at $s = s_1$, was fairly reproducible. Consequently a "master" strain pulse shape $\epsilon^*(s_1, t)$ was tabulated and used to compute the equivalent axial force loading during impact according to the relation

$$P(0, t - s_1) = A\epsilon^*(s_1, t), \qquad s_1 \leq t \leq 2s_2 - s_1, \tag{6.1}$$

which follows from the dispersionless nature of elementary longitudinal waves. In (6.1), t is measured from the moment of impact, and the relation ceases to be valid for $t > 2s_2 - s_1$ since reflections from the crack interface arrive at the monitoring station at $t = 2s_2 - s_1$. As long as the input pulse duration is less than $2(s_2 - s_1)$, (6.1) will describe the entire pulse, and it suffices to set $P(0, t - s_1) = 0$ for all t outside the indicated time range.

The experimentally determined loading condition (6.1) was used as input to the numerical solution of the equations arising from the theoretical bone model. Computed results for the surface strains at $s = s_1$ for each of the crack depths mentioned above were then superimposed in dashed curves on the respective figures.

An examination of Figs. 5–7 reveals that the theoretical predictions for surface strains at the monitoring station are in general agreement with the experimental results. Of course, for (real) time less than $(2s_2 - s_1)h/c_0$, or about 0.410 ms in this case, the two results are supposed to agree. For time greater than 0.410 ms, results will agree only if the the theoretical model of the experimental bar is appropriate.

Particular attention is directed to the results in the time interval between 0.410 ms and 0.683 ms, the latter figure being the time, in this case, at which reflections from the free end ($s = s_3$) begin to affect the gage response at $s = s_1$. It will be seen in Fig. 5 that the crack-reflected pulses monitored in this time interval are rather weak. Since the results in Fig. 5 are for a moderately deep crack, it is probable that shallow cracks (i.e. those for which $2a/h \ll 0.5$) would not be detected. On the other hand, as the crack is made deeper, the crack-reflected pulse is strengthened and becomes easily detectable. See Figs. 6 and 7. The

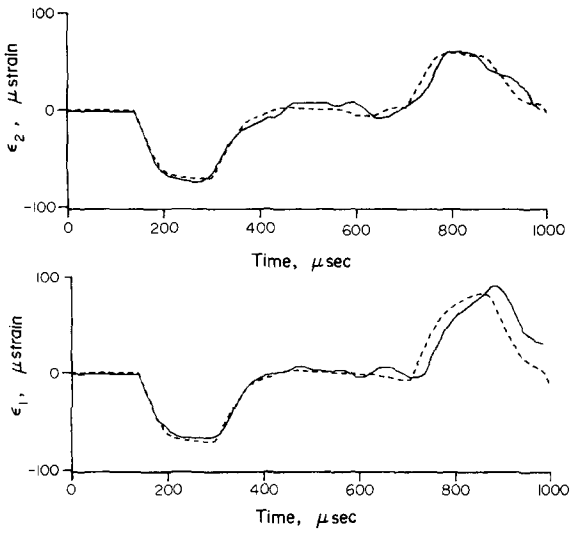

Fig. 5. Comparison between the theoretical and experimental strain gage responses for $2a/h = 0.50$. (------) Theory (——) Experiment.

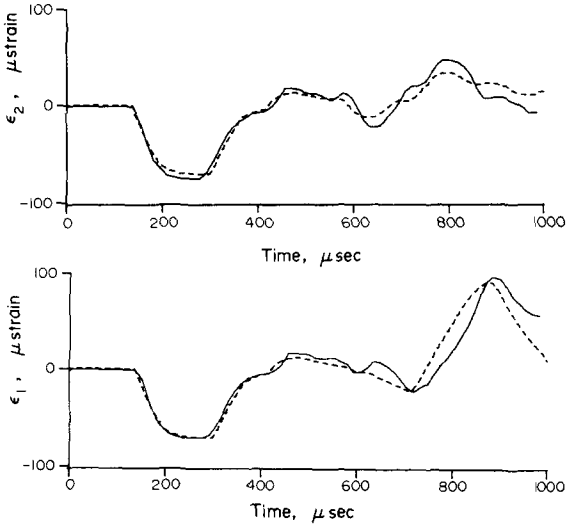

Fig. 6. Comparison between the theoretical and experimental strain gage responses for $2a/h = 0.75$. (------) Theory (——) Experiment.

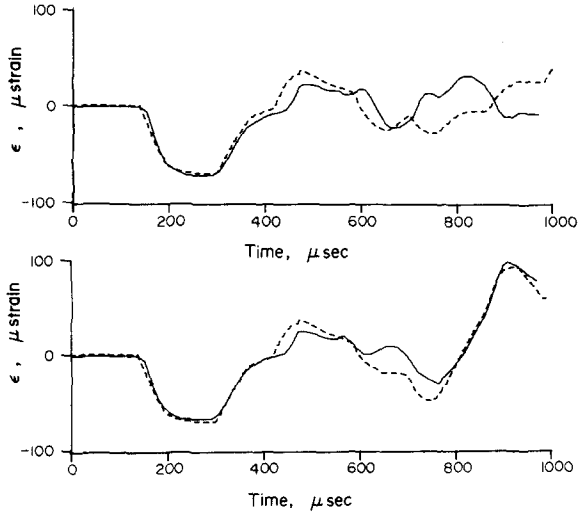

Fig. 7. Comparison between the theoretical and experimental strain gage responses for $2a/h = 0.88$. (------) Theory (——) Experiment.

limiting case of a complete fracture at $s = s_2$ would be characterized by the reflection of a purely longitudinal pulse identical to the input pulse (except for the sign).

7. CONCLUSIONS

An effort has been made to model the effect of a single transverse edge crack on the propagation of mechanical pulses in a bar. One-dimensional wave propagation theories were used, with full recognition of the fact that the crack introduces a geometric discontinuity that destroys locally the conditions favorable for the applicability of the one-dimensional theories. Nevertheless, the theoretical predictions of reflected strain pulses for all the crack depths considered agreed fairly well with the experimentally obtained strain gage records. It is conceivable that some other model of the cracked region might prove to be equally effective for the stated problem, but the compliance model developed in this paper is at least rigorous in the sense that it is based upon the two-dimensional elasticity solution for an edge crack in a strip of finite width.

The results indicate that the one-dimensional stress-wave detection of cracks is useful only for finding serious cracks, i.e. cracks having a depth of (say) one-third the bar thickness, or greater. Also, it has been assumed that the crack is opened sufficiently to prevent contact of the adjacent crack faces during passage of the strain pulse.

With regard to the possible medical application of the method in bone healing diagnosis, it can be said that the results of this work may contribute to the analysis of pulse-reflection clinical tests on partially fractured bone. This statement is made cautiously since it is generally recognized that there are many factors affecting the propagation of waves in living bone[3].

Acknowledgements—The authors' interest in this problem arose from discussions between Dr. S. Saha (Department of Engineering and Applied Science, Yale University) and one of the authors (A.F.M.). At the time this work was done, all the authors were associated with the Department of Theoretical and Applied Mechanics, University of Illinois at Urbana-Champaign. Computing services were provided by the Computing Services Office, University of Illinois at Urbana-Champaign.

REFERENCES

1. S. Saha and R. Pelker, Stress Wave propagation in bone. *Proc. 28th Annual Conf. Engng. Med. Biol.*, 172 (1975).
2. E. Buturla and M. Pope, A finite element wave propagation model of pathogenic and healing bone. *Proc. 1st New England Conf. Bioengng.* (Edited by M. H. Pope, R. W. McLay and R. G. Absher), 36–45 (1973).
3. J. L. Lewis, A dynamic model of a healing fractured long bone. *J. Biomech.* **8**, 17–25 (1975).
4. D. A. Sonstegard and L. S. Matthews, Sonic diagnosis of bone fracture healing—a preliminary study. *J. Biomech.* **9**, 689–694 (1976).
5. J. W. Phillips, Stress pulses produced during the fracture of brittle tensile specimens. *Int. J. Solids Structures* **6**, 1403–1412 (1970).
6. S. P. Timoshenko, On the correction for shear of the differential equation for transverse vibrations of prismatic bars. *Phil. Mag.* **41**, 744–746 (1921).
7. R. D. Mindlin, Influence of rotatory inertia and shear on flexural motions of isotropic elastic plates. *J. Appl. Mech.* **18**, 31–38 (1951).
8. J. D. Achenbach, *Wave Propagation in Elastic Solids*, Section 6.11. North-Holland, Amsterdam (1973).
9. J. W. Phillips and F. B. Crowley, III, On the theory of pulse propagation in curved beams. *J. Sound Vib.* **24**, 247–258 (1972). (1972).
10. F. B. Crowley, III, J. W. Phillips and C. E. Taylor, Pulse propagation in straight curved beams—theory and experiment. *J. Appl. Mech.* **41**, 71–76 (1974).
11. N. E. Ashbaugh, Stresses in laminated composites containing a broken layer. *J. Appl. Mech.* **40**, 533–540 (1973).
12. J. P. Bentham and W. T. Koiter, Asymptotic approximations to crack problems. *Methods of Analysis and Solutions of Crack Problems* (Edited by G. C. Sih). pp. 131–178. Noordhoff, Leyden (1973).
13. J. W. Dally and W. F. Riley, *Experimental Stress Analysis*, pp. 446–459. McGraw-Hill New York (1965).
14. P. C. Chou and R. W. Mortimer, Solution of one-dimensional elastic wave problems by the method of characteristics. *J. Appl. Mech.* **34**, 745–750 (1967).
15. H. J. Plass, Some solutions of the Timoshenko beam equation for short pulse-type loading. *J. Appl. Mech.* **25**, 379–385 (1958).